Received August 27, 2021, accepted September 20, 2021, date of publication September 22, 2021, date of current version October 7, 2021.

Digital Object Identifier 10.1109/ACCESS.2021.3114713

Cooperative Communications for Improving the Performance of Bidirectional Full-Duplex System With Multiple Reconfigurable Intelligent Surfaces

BA CAO NGUYEN[1], TRAN MANH HOANG[1], PHUONG T. TRAN[2], (Senior Member, IEEE), TAN N. NGUYEN[2], (Member, IEEE), VAN-DUC PHAN[3], BUI VU MINH[4], AND MIROSLAV VOZNAK[5], (Senior Member, IEEE)

[1]Faculty of Basic Techniques, Telecommunications University, Nha Trang, Khanh Hoa 65000, Vietnam
[2]Wireless Communications Research Group, Faculty of Electrical and Electronics Engineering, Ton Duc Thang University, Ho Chi Minh City 729000, Vietnam
[3]Faculty of Automobile Technology, Van Lang University, Ho Chi Minh City 72900, Vietnam
[4]Faculty of Mechanical, Electrical, Electronic and Automotive Engineering, Nguyen Tat Thanh University, Ho Chi Minh City 72900, Vietnam
[5]Faculty of Electrical Engineering and Computer Science, VSB–Technical University of Ostrava, 708 00 Ostrava, Czech Republic

Corresponding author: Tan N. Nguyen (nguyennhattan@tdtu.edu.vn)

This work was supported by the Ministry of Education, Youth and Sports of the Czech Republic under Grant SP2021/25 and Grant e-INFRA CZ (ID: 90140).

ABSTRACT In this paper, we exploit the benefits of full-duplex (FD) transmission and reconfigurable intelligent surfaces (RISs) by considering a bidirectional full-duplex wireless communication system with the support of RISs. Specifically, cooperative communications are applied at two FD terminals in a RISs-assisted bidirectional full-duplex (RIS-FD) system. In this context, we successfully derive the mathematical expressions of the outage probability (OP) and the ergodic capacity (EC) of the RIS-FD system with a direct link between two terminals and multiple reflecting paths created by RISs over the Rayleigh fading channel. Numerical results show that the performance of the considered RIS-FD system depends significantly on the total number of reflecting elements in the RISs. Particularly, when the total number of reflecting elements is small, the OP and EC saturate at a high signal-to-noise ratio (SNR). However, when the total number of reflecting elements is large enough, OP decreases greatly while EC enhances significantly. In addition, the effect of residual self-interference (SI) caused by FD transmission on OP and EC is remarkable, even the residual SI level is very small. On the other hand, the influence of other system parameters such as the number of RISs (N) and the number of reflecting elements (L) are also investigated to fully consider the performance of the RIS-FD system. An important observation is that when current techniques cannot completely eliminate SI in FD transmission, the use of multiple RISs with larger L can indirectly reduce the impact of SI and significantly improve the performance of the proposed RIS-FD system. Finally, the obtained expressions are validated via Monte-Carlo simulations.

INDEX TERMS Reconfigurable intelligent surfaces, full-duplex, outage probability, ergodic capacity.

I. INTRODUCTION

Nowadays, bidirectional full-duplex (FD) communication systems are expected to replace traditional half-duplex (HD) communication systems due to the high capacity of the FD technique. Theoretically, the FD technique doubles the spectral efficiency compared to HD counterpart [1]. However, strong self-interference (SI) from the FD terminal's output to its input is still a challenge in practical scenarios [2]. Fortunately, thanks to advantages in analog and digital signal processing as well as in antenna design, FD devices can be deployed in near future to satisfy the high capacity requirements of the fifth-generation (5G) and beyond networks [3]–[5]. Specifically, three main domains such as antenna cancellation, analog and digital suppressions are applied to suppress SI in the FD devices [1], [6]–[8]. It was shown that, after applying all SI cancellation (SIC) techniques, the residual SI power can be low as the noise floor in FD

The associate editor coordinating the review of this manuscript and approving it for publication was Eyuphan Bulut.

communications [6], [7]. Recently, various solutions and algorithms are continuously proposed to achieve better SIC before deploying FD transmission in practice [9], [10].

To demonstrate the benefits of FD transmission, many works have analyzed the performance of FD communication systems under the existence of residual SI in comparison to conventional HD communication systems. It is observed that the outage probability (OP) of the FD systems is saturated in a high signal-to-noise ratio (SNR) regime due to the effect of residual SI [11]–[14]. In addition, the ergodic capacity (EC) of the FD systems may be higher or lower than that of the HD systems [15]. This feature depends on residual SI and transmit SNR ranges. In particular, the FD systems often have a higher EC than that of the HD systems in low SNR mode and vice versa. It is because high SNR leads to high residual SI power, thus the EC of the FD system reaches the capacity floor while the EC of the HD system still increases with the increasing of SNR [16]. Furthermore, the FD transmission has been widely applied with various new techniques such as non-orthogonal multiple access, spatial modulation, energy harvesting, cooperative communication, and cognitive communications, for exploiting the advantages of these techniques [17]–[22].

Besides FD transmission, RIS has recently emerged as a promising technology since RIS can assist wireless systems to significantly enhance the coverage, the reliability, and quality-of-service [23], [24]. Thus, this technology is expected to be deployed in sixth-generation (6G) and beyond wireless systems [23], [25]. Specifically, RIS can be implemented in wireless systems such as relays but operate without decoding, encoding, or amplifying signals [24]. Therefore, the application of RIS in wireless systems can significantly reduce the system complexity compared to other techniques such as the relay. In addition, RIS can reflect the wireless signals with the desired phase shift to maximize the received signal power at the end users [23], [26]. Consequently, using RIS to support wireless communication systems becomes a potential innovative solution. Moreover, RIS can be easily integrated into existing wireless communication environments [27].

In the literature, the performance of RIS-assisted wireless systems has been analyzed in various scenarios such as over Rayleigh, Nakagami-*m* channels, ideal hardware or hardware impairments, etc. [23]–[27]. Specifically, the performance in the RIS use cases was compared with the amplify-and-forward relay [25] or decode-and-forward relay use cases [26]. It has been proven that using RIS can achieve better performance than amplify-and-forward relay even if there is only one reflecting element in RIS [25]. Meanwhile, larger reflecting elements are needed in RIS-enabled wireless system to perform better than the decode-and-forward relay system [26]. In addition, using multiple RISs in cooperative communication systems can significantly improve the performance in terms of OP and EC when the direct source-to-destination link is weak [28].

Recently, RIS has been combined with FD transmission to exploit the benefits of both techniques [20], [29]–[32]. Particularly, with the support of RIS, the bidirectional FD system can achieve higher performance than the bidirectional FD-based amplify-and-forward relaying system [32]. More importantly, using RIS with large reflecting elements can greatly reduce the impact of residual SI and subsequently improve OP and symbol error rate (SER) performance of a RSI-assisted FD system. In addition, under the support of the RIS, the FD technique could achieve better performance than the HD one [30]. Furthermore, the RIS-enabled multiple users in the FD system was also investigated in [31]. Herein, the authors demonstrated that RIS can help suppress interference in FD users via adjusting the reflecting paths between the base station and users.

As shown in the above discussions, both RIS and FD techniques are potential solutions for future wireless networks. Especially, RIS can significantly reduce the impact of residual SI in the FD systems [32]. On the other hand, most of the previous works used only one RSI in the FD systems and ignored the direct link between the two terminals [31], [32]. Meanwhile, the combination of multiple RISs and cooperative communications can greatly improve the performance of RIS-assisted FD systems. Specifically, multiple RISs can be located in different locations for reflecting signals between two FD terminals. Consequently, in the case that the signals reflected via one or two RISs are not available at the receiver, the receiver still receives the desired signals reflected via other RISs. Thus, the received signal power at the receiver in the case that multiple RISs can be significantly enhanced in comparison with the case that only one RIS. In addition, the work in [28] demonstrated that the RISs equipped with different numbers of reflecting elements can achieve better performance than the RISs equipped with similar numbers of reflecting elements in the case that the RISs are located in different locations. However, this work was considered for HD system. Furthermore, the obtained expressions with multiple RISs are more complex than those with one RIS [23], [28]. Thus, most of previous works considered only one RIS for analyzing the performance of FD systems. These problems motivate us to mathematically consider a multiple RISs-assisted FD system (hereafter referred to as RIS-FD system) in which the direct link between two FD terminals is exploited. The main contributions of this paper can be summarized as follows:

- We exploit the benefits of both FD and RIS techniques by applying them to a wireless system where cooperative communications are applied to improve performance at two FD terminals. Specifically, two FD terminals combine the signals received via the direct link and the reflecting links. Additionally, imperfect SI cancellation at the two FD terminals is considered in all investigated scenarios.
- We derive the signal-to-interference-plus-noise ratios (SINRs) of the considered RIS-FD system with residual SI in cooperative communication. We then successfully obtain the expressions of the outage probability (OP) and ergodic capacity (EC) over the Rayleigh fading channel.

All obtained expressions are validated via Monte-Carlo simulations.

- We investigate the performance in terms of OP and EC of the considered RIS-FD system under different scenarios. Particularly, OP is greatly reduced and the EC is significantly enhanced because of the cooperative communications. In the case that the total number of RIS elements is small, OP and EC reach the error floor and capacity ceiling, respectively, due to the effect of residual SI caused by FD transmission. However, when the total number of RIS elements is large enough, the impact of residual SI on the OP and EC is significantly reduced. Specifically, the OP can reach 10^{-6} at SNR $= 0$ dB with 16 RIS elements. On the other hand, the EC of the RIS-FD system is almost higher than that of the traditional RIS-HD system even with a high residual SI level, especially when the total number reflecting elements is large enough. Furthermore, the impacts of system parameters such as number of RIS, number of reflecting elements, and residual SI are also investigated.

The rest of this paper is organized as follows. Section II describes the system model of the considered RIS-FD system, where the received signals and the SINRs at the FD terminals are detaily provided. Section III presents the system performance by mathematically deriving the OP and EC expressions of the considered RIS-FD system over Rayleigh fading channel. Section IV provides the numerical results and discussions via various different scenarios. Finally, Section V concludes our works.

II. SYSTEM MODEL

The system model of the RIS-FD system is described in Fig. 1. Signals are exchanged between two terminals, i.e., A and B via direct link and the assistance of multiple RISs. As shown from Fig. 1, A and B are FD devices and equipped with an FD antenna.[1] Additionally, there are N RISs in the considered system where nth RIS is equipped with L_n reflecting elements ($n = 1, 2, \ldots, N$). Note that in practice, the RISs can be equipped with different reflecting elements, i.e., $L_i \neq L_j$ for $i \neq j$ and $i, j = 1, 2, \ldots, N$.

Due to FD transmission mode, signal exchanges between two terminals A and B are performed in only one time slot. However, this transmission mode causes strong self-interference from their output and input. Let h_{nl} be the complex channel coefficient of the desired signals from A to lth reflecting element of the nth RIS. Since reciprocal channels such as in [23], [33] are considered for the considered system, the complex channel coefficient from the lth reflecting element of the nth RIS to A is also h_{nl}. Similarly, the complex channel coefficient of the desired signals between B and the lth reflecting element of the nth RIS is g_{nl}. Meanwhile, the self-interference channels are modeled via two types: i) the first one is conventional SI that comes directly and indirectly (reflecting via trees, buildings,…, excluding the RISs) from terminal's output to its input, i.e., $\tilde{h}_{aa}$ and $\tilde{h}_{bb}$ at A and B, respectively. In other words, the first one is the SI in the FD systems without RISs; ii) the second one is the new SI including the contributions of the RISs, that comes from the terminal's output to RISs and then comes back to terminal's input, i.e., $\tilde{h}_{nl}$ and $\tilde{g}_{nl}$ at A and B, respectively. It is worthy to note that the two types of the SI above can be aggregated in only one term. However, to emphasize the SI induced by the RISs, it is often described via two terms [23]. Also, the usage of the RISs in FD systems may lead to higher SI power in comparison with the case without RISs. Furthermore, the complex channel coefficient of the direct link between A and B is denoted by h_d.

Using the representation of the complex number, we can present the complex channel coefficients as $h_d = |h_d|e^{-j\phi_d}$, $h_{nl} = |h_{nl}|e^{-j\theta_{nl}}$, and $g_{nl} = |g_{nl}|e^{-j\psi_{nl}}$, where $|h_d|$, $|h_{nl}|$, and $|g_{nl}|$ are magnitudes and ϕ_d, θ_{nl}, and ψ_{nl} are phases of h_d, h_{nl}, and g_{nl}, respectively. On the other hand, the amplitude and phase of the lth reflecting element of the nth RIS are respectively denoted by $|k_{nl}|$ and φ_{nl}. Noticing that $|k_{nl}| \in (0, 1]$ and $\{\phi_d, \theta_{nl}, \psi_{nl}, \varphi_{nl}\} \in [0, 2\pi]$. In addition, L_n denotes the number of reflecting elements of the nth RIS (S_n).

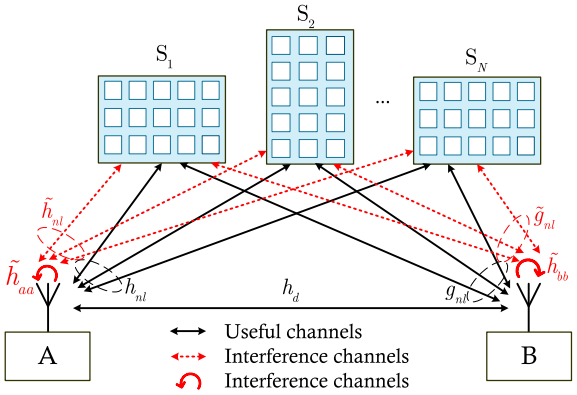

FIGURE 1. The block diagram of the RIS-FD system.

The received signals at terminals A and B of the considered RIS-FD system are, respectively, calculated as

$$y_{\mathrm{A}} = \left(h_d + \sum_{n=1}^{N}\sum_{l=1}^{L_n} g_{nl}|k_{nl}|e^{j\varphi_{nl}}h_{nl}\right)s_{\mathrm{B}} + \left(\tilde{h}_{\mathrm{aa}} + \sum_{n=1}^{N}\sum_{l=1}^{L_n}\tilde{h}_{nl}|k_{nl}|e^{j\varphi_{nl}}\tilde{h}_{nl}\right)s_{\mathrm{A}} + z_{\mathrm{A}}, \quad (1)$$

$$y_{\mathrm{B}} = \left(h_d + \sum_{n=1}^{N}\sum_{l=1}^{L_n} h_{nl}|k_{nl}|e^{j\varphi_{nl}}g_{nl}\right)s_{\mathrm{A}} + \left(\tilde{h}_{\mathrm{bb}} + \sum_{n=1}^{N}\sum_{l=1}^{L_n}\tilde{g}_{nl}|k_{nl}|e^{j\varphi_{nl}}\tilde{g}_{nl}\right)s_{\mathrm{B}} + z_{\mathrm{B}}, \quad (2)$$

[1] An FD antenna can be classified in two types, i.e., two separate antennas (one for transmitting and another for receiving) and one shared antenna (for both transmitting and receiving). Two separate antennas are often used for FD devices because this configure can help to easily deploy SIC solutions, especially in isolation techniques [1], [7], [8]. Meanwhile, shared antenna can be also used when a circulator for isolating between FD device's output and input is exploited [6], [8].

where s_A and s_B are the transmitted signals from A and B with the average transmission power of P_A and P_B, respectively; z_A and z_B are the Gaussian noises at A and B with zero mean and variance of σ^2, i.e., $z_A \sim \mathcal{CN}(0, \sigma_A^2)$ and $z_B \sim \mathcal{CN}(0, \sigma_B^2)$.

As shown from (1) and (2), the received signal expressions at A and B have a similar type. Thus, the further expressions such as SINR and OP at two terminals are also similar. Consequently, we only focus on the terminal B in the followings. The signal processing as well as other expressions at A can be easily derived from them of B.

For FD transmission mode, all SIC techniques should be applied at FD terminals to suppress the SI power. Specifically, three domains such as antenna domain, analog and digital cancellations are applied for FD devices [1], [6]–[8]. In particular, the antenna domain is used to isolate between the output signal and input signal of a FD device. In this the domain, many effective methods such as cross polarization, directional isolation, and absorptive shielding are often used [6], [7]. Then, the residual SI is canceled via analog canceller (using analog circuits) to continuously reduce the SI power [8]. Finally, the SI is suppressed in sophisticated processing in the digital domain [1], [8]. Since the three SIC domains are applied, the phase shifts induced by RISs and other objects can be completely removed because the digital-domain cancellation is carried out after a quantization operation [23], [29]. As the results, the residual SI after all SIC techniques can be considered as noise source [12], [15], [17], [34]. In other words, the terms $\left(\tilde{h}_{bb} + \sum_{n=1}^{N}\sum_{l=1}^{L_n} \tilde{g}_{nl}|k_{nl}|e^{j\varphi_{nl}}\tilde{g}_{nl}\right)s_B$ becomes a new variable I_B with zero mean and variance of $\sigma_{SI_B}^2 P_B$, i.e., $I_B \sim \mathcal{CN}(0, \sigma_{SI_B}^2 P_B)$, where $\sigma_{SI_B}^2 \in [0, 1]$ refers the residual SI level at terminal B.

Consequently, the received signal at B from (2) now becomes

$$y_B = \left(h_d + \sum_{n=1}^{N}\sum_{l=1}^{L_n} h_{nl}|k_{nl}|e^{j\varphi_{nl}}g_{nl}\right)s_A + I_B + z_B. \quad (3)$$

Now, using the amplitudes and phases of the complex channel coefficients, we can rewrite (3) as

$$y_B = \left(|h_d|e^{-j\phi_d} + \sum_{n=1}^{N}\sum_{l=1}^{L_n} |h_{nl}||k_{nl}||g_{nl}|e^{j(\varphi_{nl}-\theta_{nl}-\psi_{nl})}\right)s_A + I_B + z_B. \quad (4)$$

Then, we represent (4) as

$$y_B = e^{-j\phi_d}\left(|h_d| + \sum_{n=1}^{N}\sum_{l=1}^{L_n} |h_{nl}||k_{nl}||g_{nl}|e^{j\Delta}\right)s_A + I_B + z_B, \quad (5)$$

where $\Delta = \varphi_{nl} - \theta_{nl} - \psi_{nl} + \phi_d$ is called as phase error of the lth reflecting element of the nth RIS [28].

As presented in the literature, the phase shifts of the RISs can be reconfigured to maximize the received signal power at the terminals [23]–[26]. In particular, the phase shifts of reflecting elements rely on the diodes employed in the RISs [35], [36]. Consequently, the phase shifts may be not continuous due to the hardware limitations. Thus, the discrete phase shifts are often considered in the RIS assisted wireless communication systems [28], [36]. Therefore, the number of phase shifts is limited and constrained by a phase shift resolution [36]. Hence, the phase shift values can be uniformly mapped to the interval $[0, 2\pi)$. Let b_n and $\mathbb{Q}_n \triangleq 2^{b_n}$ be, respectively, the number of quantization bits and the phase shift resolution of the nth RIS. As the results, a phase shift value can be chosen from the following set [28], [36]

$$\mathbb{T} = \left\{0, \frac{2\pi}{\mathbb{Q}_n}, \frac{4\pi}{\mathbb{Q}_n}, \ldots, \frac{2\pi(\mathbb{Q}_n - 1)}{\mathbb{Q}_n}\right\}. \quad (6)$$

With a high phase shift resolution, i.e., $\mathbb{Q}_n \gg 1$ and the perfect channel estimations are available at the RISs, the nth RIS can generate ideal phase shifts such that the phase errors can be zero, i.e., $\Delta = 0$ [28], [29], [36]. This assumption was widely discussed in the literature and it was demonstrated that it is inline with realistic implementations [25], [36], [37]. It is worth noticing that the ideal phase shift assumption has been extensively used for single-RIS-aided systems [23], [25] and multi-RIS-aided systems [28], [29], [36]. We also note that in practice, the RIS assisted wireless communication systems are generally implemented with discrete phase shifts as they are cost-effective and easy to achieve the idea phase shifts. However, such implementation causes degradation in the performance [36].

As the results, the phase shift of the lth reflecting element of the nth RIS is reconfigured as $\varphi_{nl} = \theta_{nl} + \psi_{nl} - \phi_d$. Consequently, we have $\Delta = 0$. Therefore, the received signal at B becomes

$$y_B = e^{-j\phi_d}\left(|h_d| + \sum_{n=1}^{N}\sum_{l=1}^{L_n} |h_{nl}||k_{nl}||g_{nl}|\right)s_A + I_B + z_B. \quad (7)$$

Based on (7), the instantaneous SINR at B is calculated as

$$\gamma_B = \frac{|e^{-j\phi_d}|^2\left(|h_d| + \sum_{n=1}^{N}\sum_{l=1}^{L_n} |h_{nl}||k_{nl}||g_{nl}|\right)^2 P_A}{\sigma_{SI_B}^2 P_B + \sigma_B^2}. \quad (8)$$

Since $|e^{-j\phi_d}|^2 = 1$, the instantaneous SINR at B is now expressed as

$$\gamma_B = \frac{\left(|h_d| + \sum_{n=1}^{N}\sum_{l=1}^{L_n} |h_{nl}||k_{nl}||g_{nl}|\right)^2 P_A}{\sigma_{SI_B}^2 P_B + \sigma_B^2}. \quad (9)$$

III. PERFORMANCE ANALYSIS

A. OUTAGE PROBABILITY

The OP of the wireless systems can be calculated as the probability when the instantaneous data transmission rate drops below a pre-defined data transmission rate [38]. Mathematically, the OP of the considered RIS-FD system (denoted by $\mathcal{P}_{out}$) is given as

$$\mathcal{P}_{out} = \Pr\{\log_2(1 + \gamma_B) < \mathcal{R}\}, \quad (10)$$

where $\gamma_{\rm B}$ and $\mathcal{R}$ are respectively the instantaneous SINR (given in (9)) and the pre-data transmission rate (bit/s/Hz).

Then, (10) is rewritten as

$$\mathcal{P}_{\rm out} = \Pr\{\gamma_{\rm B} < 2^{\mathcal{R}} - 1\} = \Pr\{\gamma_{\rm B} < \gamma_{\rm th}\}, \tag{11}$$

where $\gamma_{\rm th} \triangleq 2^{\mathcal{R}} - 1$ is defined as the SINR threshold.

Substituting $\gamma_{\rm B}$ from (9) into (11), the OP is now calculated as

$$\mathcal{P}_{\rm out} = \Pr\left\{ \frac{\left(|h_d| + \sum_{n=1}^{N}\sum_{l=1}^{L_n} |h_{nl}||k_{nl}||g_{nl}|\right)^2 P_{\rm A}}{\sigma_{\rm SI_B}^2 P_{\rm B} + \sigma_{\rm B}^2} < \gamma_{\rm th} \right\}. \tag{12}$$

Then, we rewrite (12) as

$$\mathcal{P}_{\rm out} = \Pr\left\{ \mathcal{Z}^2 < \frac{(\sigma_{\rm SI_B}^2 P_{\rm B} + \sigma_{\rm B}^2)\gamma_{\rm th}}{P_{\rm A}} \right\}. \tag{13}$$

where $\mathcal{Z} = |h_d| + \mathcal{T}$, $\mathcal{T} = \sum_{n=1}^{N} \mathcal{V}_n$, $\mathcal{V}_n = \sum_{l=1}^{L_n} \mathcal{U}_{nl}$, $\mathcal{U}_{nl} = |h_{nl}||k_{nl}||g_{nl}|$.

From (13), the OP of the RIS-FD system is computed in the following Theorem 1.

Theorem 1: The OP of the RIS-FD system with cooperative communication is given by

$$\mathcal{P}_{\rm out} = 1 - \frac{\Gamma\left(\Psi, \Theta\sqrt{\frac{(\sigma_{\rm SI_B}^2 P_{\rm B} + \sigma_{\rm B}^2)\gamma_{\rm th}}{P_{\rm A}}}\right)}{\Gamma(\Psi)}, \tag{14}$$

where $\Gamma(.)$ and $\Gamma(.,.)$ are, respectively, the gamma and the upper incomplete gamma functions;

$$\Psi = \frac{[\Xi_{\mathcal{Z}}(1)]^2}{\Xi_{\mathcal{Z}}(2) - [\Xi_{\mathcal{Z}}(1)]^2}, \tag{15}$$

$$\Theta = \frac{\Xi_{\mathcal{Z}}(1)}{\Xi_{\mathcal{Z}}(2) - [\Xi_{\mathcal{Z}}(1)]^2}, \tag{16}$$

$$\Xi_{\mathcal{Z}}(1) = \Gamma\left(\frac{3}{2}\right) + \Xi_{\mathcal{T}}(1), \tag{17}$$

$$\Xi_{\mathcal{Z}}(2) = \Gamma(2) + \Xi_{\mathcal{T}}(2) + 2\Gamma\left(\frac{3}{2}\right)\Xi_{\mathcal{T}}(1), \tag{18}$$

$$\Xi_{\mathcal{T}}(1) = \sum_{n=1}^{N}\sum_{l=1}^{L_n} \Xi_{\mathcal{U}_{nl}}(1), \tag{19}$$

$$\Xi_{\mathcal{T}}(2) = \sum_{n=1}^{N}\left[\sum_{l=1}^{L_n} \Xi_{\mathcal{U}_{nl}}(2) + 2\sum_{l=1}^{L_n} \Xi_{\mathcal{U}_{nl}}(1) \sum_{l'=l+1}^{L_n} \Xi_{\mathcal{U}_{nl'}}(1)\right] + 2\sum_{n=1}^{N}\left[\sum_{l=1}^{L_n} \Xi_{\mathcal{U}_{nl}}(1)\right] \sum_{n'=n+1}^{N}\left[\sum_{l=1}^{L_{n'}} \Xi_{\mathcal{U}_{n'l}}(1)\right], \tag{20}$$

$$\Xi_{\mathcal{U}_{nl}}(i) = |k_{nl}|^i \Gamma^2\left(1 + \frac{i}{2}\right). \tag{21}$$

Proof: To derive the OP of the considered RIS-FD system in (14), we have to obtain the cumulative distribution function (CDF) of $\mathcal{Z}^2$. Applying [28, Eq. (20)], the CDF of $\mathcal{Z}^2$, denoted by $F_{\mathcal{Z}^2}(x)$, is given as

$$F_{\mathcal{Z}^2}(x) \approx \frac{\gamma\left(\Psi, \Theta\sqrt{x}\right)}{\Gamma(\Psi)}. \tag{22}$$

Then, applying $\Gamma(a,x) + \gamma(a,x) = \Gamma(a)$, whereas $\gamma(.,.)$ is the lower incomplete gamma function, (22) is rewritten as

$$F_{\mathcal{Z}^2}(x) \approx 1 - \frac{\Gamma\left(\Psi, \Theta\sqrt{x}\right)}{\Gamma(\Psi)}. \tag{23}$$

Now, the OP is calculated as

$$\begin{aligned}\mathcal{P}_{\rm out} &= \Pr\left\{ \mathcal{Z}^2 < \frac{(\sigma_{\rm SI_B}^2 P_{\rm B} + \sigma_{\rm B}^2)\gamma_{\rm th}}{P_{\rm A}} \right\} \\ &= F_{\mathcal{Z}^2}\left(\frac{(\sigma_{\rm SI_B}^2 P_{\rm B} + \sigma_{\rm B}^2)\gamma_{\rm th}}{P_{\rm A}}\right) \\ &= 1 - \frac{\Gamma\left(\Psi, \Theta\sqrt{\frac{(\sigma_{\rm SI_B}^2 P_{\rm B} + \sigma_{\rm B}^2)\gamma_{\rm th}}{P_{\rm A}}}\right)}{\Gamma(\Psi)}.\end{aligned} \tag{24}$$

The proof is thus complete.

B. ERGODIC CAPACITY

The EC of the considered RIS-FD system is expressed as

$$\begin{aligned}\mathcal{E} &= \mathbb{E}\left\{\log_2(1+\gamma_{\rm A})\right\} + \mathbb{E}\left\{\log_2(1+\gamma_{\rm B})\right\} \\ &= \int_0^{\infty} \log_2(1+x) f_{\gamma_{\rm A}}(x)dx + \int_0^{\infty} \log_2(1+x) f_{\gamma_{\rm B}}(x)dx,\end{aligned} \tag{25}$$

where $\mathbb{E}$ is the expectation operator; $\gamma_{\rm A}$ and $\gamma_{\rm B}$ are, respectively, the SINRs at A and B; $f(.)$ is the probability density function (PDF) of the SINR.

Based on (25), the EC of the considered RIS-FD system is given in the following Theorem 2.

Theorem 2: The EC of the considered RIS-FD system is given by

$$\mathcal{E} \approx \frac{2^{\Psi}}{\sqrt{\pi}\Gamma(\Psi)\ln 2} G_{3,5}^{5,3}\left(\frac{\Theta^2(\sigma_{\rm SI_B}^2 P_{\rm B} + \sigma_{\rm B}^2)}{4 P_{\rm A}}\Big|_{\frac{\Psi}{2}, \frac{\Psi+1}{2}, 0, \frac{1}{2}, 0}^{0, \frac{1}{2}, 1}\right), \tag{26}$$

where G is the Meijer function [39].

Proof: The EC from (25) can be calculated as

$$\mathcal{E} = \frac{1}{\ln 2}\int_0^{\infty} \frac{1 - F_{\gamma_{\rm A}}(x)}{1+x}dx + \frac{1}{\ln 2}\int_0^{\infty} \frac{1 - F_{\gamma_{\rm B}}(x)}{1+x}dx. \tag{27}$$

Without loss of generality, we assume that the two terminals A and B have similar parameters (symmetric model). Thus, we have $F_{\gamma_{\rm A}}(x) = F_{\gamma_{\rm B}}(x)$. Therefore, (27) becomes

$$\mathcal{E} = \frac{2}{\ln 2}\int_0^{\infty} \frac{1 - F_{\gamma_{\rm B}}(x)}{1+x}dx. \tag{28}$$

To derive the EC, we firstly obtain the CDF, i.e., $F_{\mathrm{B}}(x)$. Mathematically, $F_{\mathrm{B}}(x)$ is computed as

$$F_{\gamma_{\mathrm{B}}}(x) = \Pr\{\gamma_{\mathrm{B}} < x\}. \tag{29}$$

Thus, we have

$$F_{\gamma_{\mathrm{B}}}(x) = 1 - \frac{\Gamma\left(\Psi, \Theta\sqrt{\frac{(\sigma_{\mathrm{SI_B}}^2 P_{\mathrm{B}} + \sigma_{\mathrm{B}}^2)x}{P_{\mathrm{A}}}}\right)}{\Gamma(\Psi)}. \tag{30}$$

Substituting the CDF from (30) into (28), we can calculate the EC as

$$\mathcal{E} = \frac{2}{\Gamma(\Psi)\ln 2}\int_0^{\infty} \frac{\Gamma\left(\Psi, \Theta\sqrt{\frac{(\sigma_{\mathrm{SI_B}}^2 P_{\mathrm{B}} + \sigma_{\mathrm{B}}^2)x}{P_{\mathrm{A}}}}\right)}{1+x} dx. \tag{31}$$

Applying [40, Eq. (8.4.2.5)], the term $(1+x)^{-1}$ in (31) is expressed as

$$(1+x)^{-1} = G_{1,1}^{1,1}\left(x\middle|_{0}^{0}\right). \tag{32}$$

On the other hand, applying [40, Eq. (8.4.16.2)], we can represent the gamma function as

$$\Gamma\left(\Psi, \Theta\sqrt{\frac{(\sigma_{\mathrm{SI_B}}^2 P_{\mathrm{B}} + \sigma_{\mathrm{B}}^2)x}{P_{\mathrm{A}}}}\right) = G_{1,2}^{2,0}\left(\Theta\sqrt{\frac{(\sigma_{\mathrm{SI_B}}^2 P_{\mathrm{B}} + \sigma_{\mathrm{B}}^2)x}{P_{\mathrm{A}}}}\middle|_{\Psi,0}^{1}\right). \tag{33}$$

Then, the EC is expressed as

$$\mathcal{E} = \frac{2}{\Gamma(\Psi)\ln 2}\int_0^{\infty} G_{1,1}^{1,1}\left(x\middle|_{0}^{0}\right) \times G_{1,2}^{2,0}\left(\Theta\sqrt{\frac{(\sigma_{\mathrm{SI_B}}^2 P_{\mathrm{B}} + \sigma_{\mathrm{B}}^2)}{P_{\mathrm{A}}}x^{\frac{1}{2}}}\middle|_{\Psi,0}^{1}\right) dx. \tag{34}$$

Applying [40, Eq. (2.24.1.1)], the integral in (34) is solved as

$$\int_0^{\infty} G_{1,1}^{1,1}\left(x\middle|_{0}^{0}\right) G_{1,2}^{2,0}\left(\Theta\sqrt{\frac{(\sigma_{\mathrm{SI_B}}^2 P_{\mathrm{B}} + \sigma_{\mathrm{B}}^2)}{P_{\mathrm{A}}}x^{\frac{1}{2}}}\middle|_{\Psi,0}^{1}\right) dx = \frac{2^{\Psi-1}}{\sqrt{\pi}} G_{3,5}^{5,3}\left(\frac{\Theta^2(\sigma_{\mathrm{SI_B}}^2 P_{\mathrm{B}} + \sigma_{\mathrm{B}}^2)}{4\,P_{\mathrm{A}}}\middle|_{\frac{\Psi}{2}, \frac{\Psi+1}{2}, 0, \frac{1}{2}, 0}^{0, \frac{1}{2}, 1}\right). \tag{35}$$

Replacing (35) into (34), we obtain the EC of the considered RIS-FD system as (26) in the Theorem 2. This ends the proof.

IV. NUMERICAL RESULTS AND DISCUSSIONS

In this section, the obtained mathematical expressions in previous section are used to evaluate the performance of the considered RIS-FD system. Monte-Carlo simulation results are provided to validate the numerical results. Specifically, we use MATLAB software with 10^7 channel realizations to obtain the simulation results. Similar to works in [23]–[25], [27], [29], we normalize the distances from A to the RISs and from the RISs to B. It is worth noticing that the parameter settings may be set as [41], [42] where the certainly practical scenarios are considered. In all scenarios, the system parameters are set as follows: the average transmission power and the variances of Gaussian noises of A and B are $P_{\mathrm{A}} = P_{\mathrm{B}} = P$ and $\sigma_{\mathrm{A}}^2 = \sigma_{\mathrm{B}}^2 = \sigma^2$, respectively; the residual SI levels are $\sigma_{\mathrm{SI_A}}^2 = \sigma_{\mathrm{SI_B}}^2 = \sigma_{\mathrm{SI}}^2$; and the average SNR is computed as $\mathrm{SNR} = P/\sigma^2$.

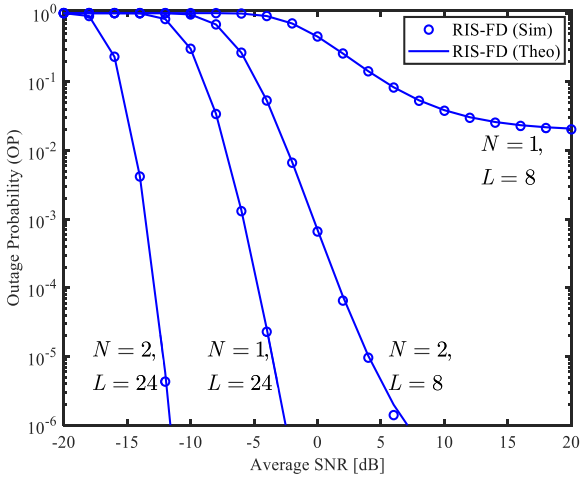

FIGURE 2. The OP of the considered RIS-FD system versus the average SNR for different values of N and L_n, i.e., $N = 1, L = 8$; $N = 1, L = 24$; $N = 2, L = 8$; $N = 2, L = 24$; $\mathcal{R} = 5$ bit/s/Hz; $\sigma_{\mathrm{SI}}^2 = 0.5$.

Fig. 2 illustrates the OP of the considered RIS-FD system versus the average SNR for different values of N and L_n, i.e., $N = 1, L = 8$; $N = 1, L = 24$; $N = 2, L = 8$; $N = 2, L = 24$. The pre-defined data transmission rate is $\mathcal{R} = 5$ bit/s/Hz and the residual SI level is $\sigma_{\mathrm{SI}}^2 = 0.5$. We use (14) to plot the theory curves of the OP while the markers "$\circ$" denote the Monte-Carlo simulation results. As shown from Fig. 2, in the case of $N = 1, L = 8$, the performance of the considered RIS-FD system is significantly impacted by the residual SI, especially in high SNR regime. In particular, the OP seems to reach the error floor at SNR = 20 dB. This result is reasonable due to the fact that the power of residual SI increases when SNR increases. Thus, higher SNR leads to higher residual SI power. Hence, the SINR (refers to (9)) slightly increases when SNR increases in high SNR regime. However, for higher value of L or N, i.e., $N = 1, L = 24$, $N = 2, L = 8$, and $N = 2, L = 24$, the OPs are greatly reduced in comparison with the case that $N = 1, L = 8$. In the these cases, the channel gains between two terminals are enhanced significantly due to the existences of many reflecting elements. In other words, the term $\mathcal{Z}$ is larger for larger N and L leading to the SINRs at terminals rapidly increase. Therefore, the performance of the considered RIS-FD system is greatly improved. Another important observation from Fig. 2 is that the OPs can avoid the error floor in the cases of $N = 1, L = 24$, $N = 2, L = 8$,

and $N = 2, L = 24$ for the considered residual SI. As a result, when the residual SI is strong, we can use larger RISs for reducing the impact of the residual SI and improving the system performance of the RIS-FD system.[2]

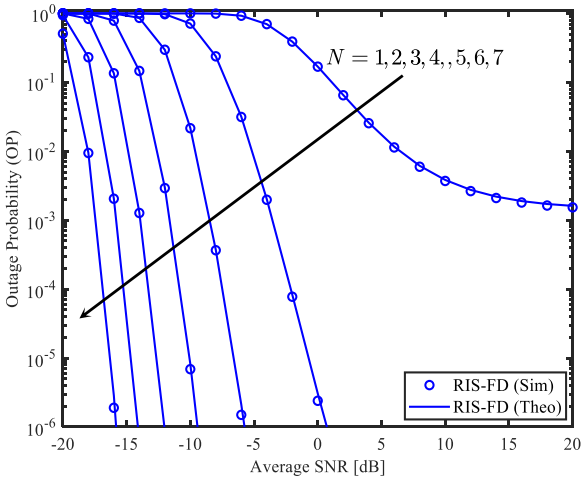

FIGURE 3. The impacts of the number of the RISs on the OP of the considered RIS-FD system, $N = 1, 2, 3, 4, 5, 6, 7$; $L = 10$; $\mathcal{R} = 5$ bit/s/Hz; $\sigma_{\text{SI}}^2 = 0.5$.

Fig. 3 investigates the impacts of the number of the RISs on the OP of the considered RIS-FD system, i.e., $N = 1, 2, 3, 4, 5, 6, 7$, where each RIS has $L = 10$ reflecting elements. It is obvious from Fig. 3 that increasing the number of the RISs greatly reduces the OP of the considered system. Specifically, in the case that $N = 1$ the OP is approximate 10^0 at SNR = 0 dB and nearly reduces to 10^{-3} at SNR = 20 dB. However, when N increases, i.e., $N = 2$, the OP is rapidly reduced. In this the case the OP is approximate 10^{-6} at SNR = 0 dB. As the results, when the total number of reflecting elements increases to twice (from 10 reflecting elements to 20 reflecting elements), the OP is approximately reduced 10^{-6} times. When N continuously increases, the OP is continuously reduced. Particularly, the OPs reach 10^{-6} for SNR $= -6, -9, -12, -14$, and -16 dB corresponding to $N = 3, 4, 5, 6$, and 7. Hence, we can use lager number of reflecting elements with a RIS or multiple RISs for improving the performance of the considered RIS-FD system. On the other hand, we shown from Fig. 2 and Fig. 3 that the diversity order of the considered RIS-FD system is a linear function of the total number of reflecting elements in the RISs.

Fig. 4 considers the impact of residual SI on the OP of the considered RIS-FD system for different values of L, i.e., $L = 2, 6, 10, 14, 18$; $N = 1$, $\mathcal{R} = 5$ bit/s/Hz, and SNR = 20 dB. In Fig. 4, the case of $\sigma_{\text{SI}}^2 = 0$ means that the terminals completely remove the SI. Meanwhile, the case of $\sigma_{\text{SI}}^2 = 1$ indicates that the terminals do not apply any SIC solutions. As can be seen from Fig. 4, the residual SI greatly impacts on

[2]It is better to note that, in the case of $N \geq 2$ and the RISs are located in different locations, the performance of the RIS system with $L_i \neq L_j$ $(i \neq j)$ may be better or worse than that of $L_i = L_j$ [28]. This result depends on the certain locations of the RISs.

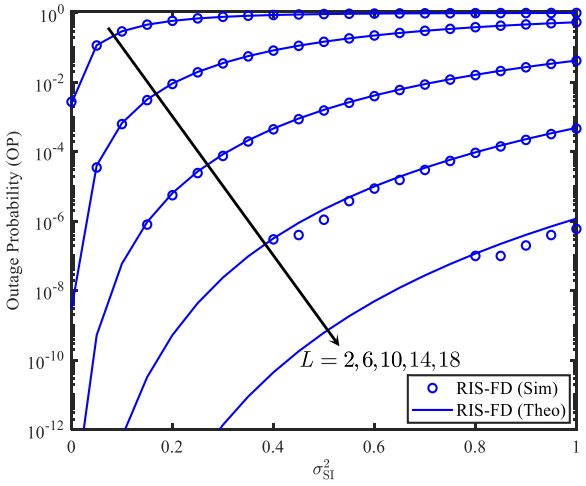

FIGURE 4. The impacts of the residual SI on the OP of the considered RIS-FD system for different values of L, i.e., $L = 2, 6, 10, 14, 18$; $N = 1$, $\mathcal{R} = 5$ bit/s/Hz, and SNR = 20 dB.

the OP even small σ_{SI}^2. Specifically, when σ_{SI}^2 increases from 0 to 0.05, the OPs increase from 3×10^{-9} and 2.5×10^{-3} to 3.5×10^{-5} and 10^{-1} for $L = 6$ and 2, respectively. As the results, for this range of the residual SI ($\sigma_{\text{SI}}^2 \in [0, 0.05]$), the OPs increase faster for higher L, i.e., the OPs increase 1.2×10^4 and 40 times for $L = 6$ and 2, respectively. When σ_{SI}^2 increases to the higher values, the OPs with small L ($L = 2, 6$) reach the error floor, especially in the case that $\sigma_{\text{SI}}^2 = 1$. On the other hand, although larger value of L significantly reduce the OP, the curve features of the OP is still similar to that in the case of small value of L. For example, the OP curves in the cases that $L = 10$, 14, and 18 are nearly parallel. Consequently, larger L will greatly reduce the OP but the impact of the residual SI is still characterized as small L.

Fig. 5 shows the EC of the considered RIS-FD system in comparison with that of the RIS-HD system for $\sigma_{\text{SI}}^2 = 0.5$, $N = 3$, and $L = 2, 4, 8, 16, 32$. The theory curves of the EC are plotted by using (26) in the Theorem 2. Unlike the OPs in Fig. 2 and Fig. 3, the ECs in Fig. 5 are saturated in high SNR regime even larger values of L, i.e., $L = 32$. As can be seen from Fig. 5, the ECs of the RIS-FD system may be higher or lower than those of the RIS-HD system. In particular, in the case of $L = 2$, the EC of the RIS-FD system is higher for SNR $<$ 20 dB and lower for SNR $>$ 20 dB than that of the RIS-HD system. For higher L, this feature is still similar, but in higher SNR value, i.e., the EC of the RIS-FD system is higher for SNR $<$ 26 dB and lower for SNR $>$ 26 dB than that of the RIS-HD system corresponding $L = 4$. These results are reasonable because high SNR leads to high residual SI in the RIS-FD system. However, with larger L, i.e., $L = 8$ or 16 or 32, the EC of the RIS-FD system is higher than that of the RIS-HD system for investigated SNR range. Hence, to achieve higher capacity than the HD ones, we should use low transmission power at the FD terminals to reduce the impact of residual SI when the number of reflecting elements

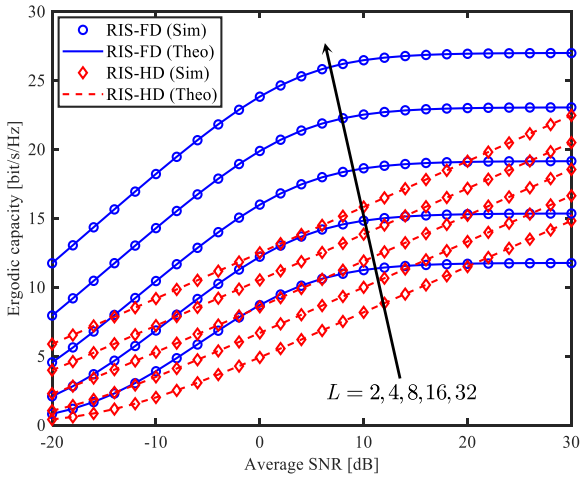

FIGURE 5. The ergodic capacity of the considered RIS-FD system in comparison with that of the RIS-HD system for $\sigma_{\text{SI}}^2 = 0.5$; $N = 3$; $L = 2, 4, 8, 16, 32$.

is small. Meanwhile, we can use high transmission power at the FD terminals when the number of reflecting elements in the RISs is large enough.

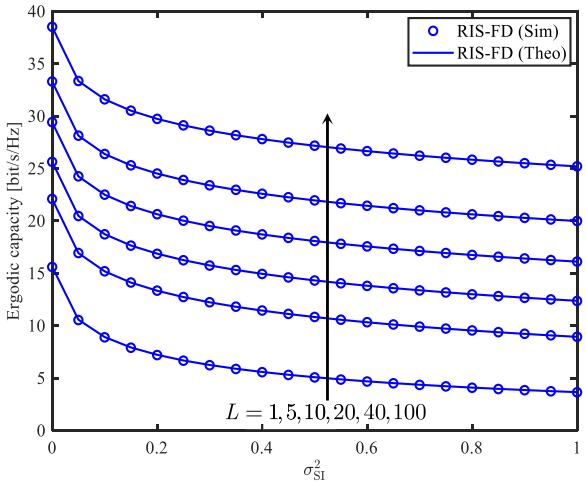

FIGURE 6. The EC of the considered RIS-FD system versus the residual SI for $N = 1$; $L = 1, 5, 10, 20, 40$, and 100.

Fig. 6 illustrates the impact of residual SI on the ECs of the considered RIS-FD system for $N = 1$; $L = 1, 5, 10, 20, 40$, and 100. It is also noted that, in the case of $\sigma_{\text{SI}}^2 = 0$ (perfect SIC) the ECs of the considered RIS-FD system are double in comparison with the ECs of the RIS-HD system. As shown in Fig. 6, the ECs decrease when σ_{SI}^2 increases. Specifically, the ECs reduce from 15.6, 22.1, 25.6, 29.4, 33.3, and 38.5 to 3.7, 8.9, 12.4, 16.1, 20, and 25.2 bit/s/Hz corresponding to $L = 1, 5, 10, 20, 40$, and 100 when σ_{SI}^2 increases from 0 to 1. In other words, the ECs reduce 11.9, 13.2, 13.2, 13.3, 13.3, and 13.3 bit/s/Hz corresponding to $L = 1, 5, 10, 20, 40$, and 100 when σ_{SI}^2 increases from 0 to 1. On the other hand, the ECs are rapidly reduced for low σ_{SI}^2 regime, i.e., $\sigma_{\text{SI}}^2 \in [0, 0.05]$, and slowly reduced for high σ_{SI}^2 regime, i.e., $\sigma_{\text{SI}}^2 \in [0.5, 1]$. In addition, larger L significantly enhance the EC of the considered RIS-FD system. Particularly, the EC increases from 7.2 ($L = 1$) to 29.7 ($L = 100$) bit/s/Hz for $\sigma_{\text{SI}}^2 = 0.2$. As the results, we can use larger L in the considered RIS-FD system to achieve higher EC and lower OP when deploying the system in practice.

V. CONCLUSION

Exploiting multiple RISs to improve wireless communication system performance and coverage is inevitable in future wireless networks. Since using RISs and FD has many advantages, especially in terms of capacity, in this paper, we have analyzed the OP and EC of a bidirectional FD system with the assistance of multiple RISs. We derived the expressions of OP and EC of the RIS-FD system with cooperative communication under the effect of residual self-interference over the Rayleigh fading channel. Numerical results indicated that, for a small number of RIS elements, OP and EC are greatly influenced by residual SI. Thus, the OP and EC reach saturation values in high SNR regime. In addition, EC may be higher or lower than that of the RIS-HD system. This feature depends on a certain value of residual SI and the number of reflecting elements. For larger numbers of reflecting elements and RISs, OP is greatly reduced and the EC significantly enhanced. Furthermore, we observed that the diversity order was a linear function of the total number of reflecting elements. From our results, we showed that when residual SI is strong at the FD terminals, we can use larger RISs to reduce its impact and significantly improve the performance.

REFERENCES

[1] E. Ahmed and A. M. Eltawil, "All-digital self-interference cancellation technique for full-duplex systems," *IEEE Trans. Wireless Commun.*, vol. 14, no. 7, pp. 3519–3532, Jul. 2015.
[2] B. C. Nguyen, L. T. Dung, T. M. Hoang, X. N. Tran, and T. Kim, "Impacts of imperfect CSI and transceiver hardware noise on the performance of full-duplex DF relay system with multi-antenna terminals over Nakagami-m fading channels," *IEEE Trans. Commun.*, early access, Jul. 26, 2021, doi: 10.1109/TCOMM.2021.3100504.
[3] K. A. Darabkh, O. M. Amro, H. B. Salameh, and R. T. Al-Zubi, "A–Z overview of the in-band full-duplex cognitive radio networks," *Comput. Commun.*, vol. 145, pp. 66–95, Sep. 2019.
[4] M. Dibaei and A. Ghaffari, "Full-duplex medium access control protocols in wireless networks: A survey," *Wireless Netw.*, vol. 26, no. 4, pp. 2825–2843, 2020.
[5] A. H. Gazestani, S. A. Ghorashi, B. Mousavinasab, and M. Shikh-Bahaei, "A survey on implementation and applications of full duplex wireless communications," *Phys. Commun.*, vol. 34, pp. 121–134, Jun. 2019.
[6] D. Bharadia, E. Mcmilin, and S. Katti, "Full duplex radios," in *Proc. ACM SIGCOMM Conf. SIGCOMM*, D. M. Chiu, J. Wang, P. Barford, and S. Seshan, Eds., Hong Kong, Aug. 2013, pp. 375–386.
[7] E. Everett, A. Sahai, and A. Sabharwal, "Passive self-interference suppression for full-duplex infrastructure nodes," *IEEE Trans. Wireless Commun.*, vol. 13, no. 2, pp. 680–694, Jan. 2014.
[8] A. Sabharwal, P. Schniter, D. Guo, D. W. Bliss, S. Rangarajan, and R. Wichman, "In-band full-duplex wireless: Challenges and opportunities," *IEEE J. Sel. Areas Commun.*, vol. 32, no. 9, pp. 1637–1652, Sep. 2014.
[9] L. Irio and R. Oliveira, "Distribution of the residual self-interference power in in-band full-duplex wireless systems," *IEEE Access*, vol. 7, pp. 57516–57526, 2019.
[10] L. G. Ordóñez, P. Ferrand, M. Duarte, M. Guillaud, and G. Yang, "On full-duplex radios with modulo-ADCs," *IEEE Open J. Commun. Soc.*, vol. 2, pp. 1279–1297, 2021.

[11] D. Choi and J. H. Lee, "Outage probability of two-way full-duplex relaying with imperfect channel state information" *IEEE Commun. Lett.*, vol. 18, no. 6, pp. 933–936, Jun. 2014.
[12] C. Li, B. Xia, S. Shao, Z. Chen, and Y. Tang, "Multi-user scheduling of the full-duplex enabled two-way relay systems," *IEEE Trans. Wireless Commun.*, vol. 16, no. 2, pp. 1094–1106, Feb. 2017.
[13] E. Fidan and O. Kucur, "Performance of transceiver antenna selection in two way full-duplex relay networks over Rayleigh fading channels," *IEEE Trans. Veh. Technol.*, vol. 67, no. 7, pp. 5909–5921, Jul. 2018.
[14] B. C. Nguyen, T. M. Hoang, and P. T. Tran, "Improving the performance of spatial modulation full-duplex relaying system with hardware impairment using transmit antenna selection," *IEEE Access*, vol. 8, pp. 20191–20202, 2020.
[15] B. C. Nguyen, X. N. Tran, D. T. Tran, X. N. Pham, and L. T. Dung, "Impact of hardware impairments on the outage probability and ergodic capacity of one-way and two-way full-duplex relaying systems," *IEEE Trans. Veh. Technol.*, vol. 69, no. 8, pp. 8555–8567, Aug. 2020.
[16] J. Feng, S. Ma, G. Yang, and H. V. Poor, "Impact of antenna correlation on full-duplex two-way massive MIMO relaying systems," *IEEE Trans. Wireless Commun.*, vol. 17, no. 6, pp. 3572–3587, Jun. 2018.
[17] Y. Alsaba, C. Y. Leow, and S. K. A. Rahim, "Full-duplex cooperative non-orthogonal multiple access with beamforming and energy harvesting," *IEEE Access*, vol. 6, pp. 19726–19738, 2018.
[18] A. Koç, I. Altunbas, and E. Basar, "Two-way full-duplex spatial modulation systems with wireless powered AF relaying," *IEEE Wireless Commun. Lett.*, vol. 7, no. 3, pp. 444–447, Jun. 2018.
[19] Q. Liang and Y. Hua, "Optimal power allocation for cooperative multiple access with non-ideal full-duplex sources," *IEEE Trans. Commun.*, vol. 69, no. 4, pp. 2372–2386, Apr. 2021.
[20] D. Xu, X. Yu, Y. Sun, D. W. K. Ng, and R. Schober, "Resource allocation for IRS-assisted full-duplex cognitive radio systems," *IEEE Trans. Commun.*, vol. 68, no. 12, pp. 7376–7394, Dec. 2020.
[21] T. M. Hoang, X. N. Tran, B. C. Nguyen, and L. T. Dung, "On the performance of MIMO full-duplex relaying system with SWIPT under outdated CSI," *IEEE Trans. Veh. Technol.*, vol. 69, no. 12, pp. 15580–15593, Dec. 2020.
[22] T. M. Hoang, B. C. Nguyen, N. N. Thang, M. Tran, and P. T. Tran, "Performance and optimal analysis of time-switching energy harvesting protocol for MIMO full-duplex decode-and-forward wireless relay networks with various transmitter and receiver diversity techniques," *J. Franklin Inst.*, vol. 357, no. 17, pp. 13205–13230, Nov. 2020.
[23] S. Atapattu, R. Fan, P. Dharmawansa, G. Wang, J. Evans, and T. A. Tsiftsis, "Reconfigurable intelligent surface assisted two-way communications: Performance analysis and optimization," *IEEE Trans. Commun.*, vol. 68, no. 10, pp. 6552–6567, Oct. 2020.
[24] E. Basar, M. Di Renzo, J. De Rosny, M. Debbah, M. Alouini, and R. Zhang, "Wireless communications through reconfigurable intelligent surfaces," *IEEE Access*, vol. 7, pp. 116753–116773, 2019.
[25] A.-A.-A. Boulogeorgos and A. Alexiou, "Performance analysis of reconfigurable intelligent surface-assisted wireless systems and comparison with relaying," *IEEE Access*, vol. 8, pp. 94463–94483, 2020.
[26] E. Björnson, O. Özdogan, and E. G. Larsson, "Intelligent reflecting surface versus decode-and-forward: How large surfaces are needed to beat relaying?" *IEEE Wireless Commun. Lett.*, vol. 9, no. 2, pp. 244–248, Feb. 2020.
[27] M. H. N. Shaikh, V. A. Bohara, A. Srivastava, and G. Ghatak, "Performance analysis of intelligent reflecting surface-assisted wireless system with non-ideal transceiver," *IEEE Open J. Commun. Soc.*, vol. 2, pp. 671–686, 2021.
[28] T. Do, G. Kaddoum, T. L. Nguyen, D. B. da Costa, and Z. J. Haas, "Multi-RIS-aided wireless systems: Statistical characterization and performance analysis," *CoRR*, vol. abs/2104.01912, pp. 1–16, Apr. 2021.
[29] P. K. Sharma and P. Garg, "Intelligent reflecting surfaces to achieve the full-duplex wireless communication," *IEEE Commun. Lett.*, vol. 25, no. 2, pp. 622–626, Feb. 2021.
[30] Y. Cai, M. Zhao, K. Xu, and R. Zhang, "Intelligent reflecting surface aided full-duplex communication: Passive beamforming and deployment design," *CoRR*, vol. abs/2012.07218, pp. 1–30, Dec. 2020.
[31] Z. Peng, Z. Zhang, C. Pan, L. Li, and A. L. Swindlehurst, "Multiuser full-duplex two-way communications via intelligent reflecting surface," *IEEE Trans. Signal Process.*, vol. 69, pp. 837–851, 2021.
[32] B. C. Nguyen, T. M. Hoang, L. T. Dung, and T. Kim, "On performance of two-way full-duplex communication system with reconfigurable intelligent surface," *IEEE Access*, vol. 9, pp. 81274–81285, 2021.
[33] H. Cui, M. Ma, L. Song, and B. Jiao, "Relay selection for two-way full duplex relay networks with amplify-and-forward protocol," *IEEE Trans. Wireless Commun.*, vol. 13, no. 7, pp. 3768–3777, Jul. 2014.
[34] C. Li, Z. Chen, Y. Wang, Y. Yao, and B. Xia, "Outage analysis of the full-duplex decode-and-forward two-way relay system," *IEEE Trans. Veh. Technol.*, vol. 66, no. 5, pp. 4073–4086, May 2017.
[35] Q. Q. Wu and R. Zhang, "Beamforming optimization for wireless network aided by intelligent reflecting surface with discrete phase shifts," *IEEE Trans. Commun.*, vol. 68, no. 3, pp. 1838–1851, May 2020.
[36] T. Hou, Y. Liu, Z. Song, X. Sun, and Y. Chen, "MIMO-NOMA networks relying on reconfigurable intelligent surface: A signal cancellation-based design," *IEEE Trans. Commun.*, vol. 68, no. 11, pp. 6932–6944, Nov. 2020.
[37] V. S. Asadchy, M. Albooyeh, S. N. Tcvetkova, A. Díaz-Rubio, Y. Ra'di, and S. A. Tretyakov, "Perfect control of reflection and refraction using spatially dispersive metasurfaces," *Phys. Rev. B, Condens. Matter*, vol. 94, no. 7, 2016, Art. no. 075142.
[38] A. Goldsmith, *Wireless Communications*. Cambridge, U.K.: Cambridge Univ. Press, 2005.
[39] A. Jeffrey and D. Zwillinger, *Table of Integrals, Series, and Products*. New York, NY, USA: Academic, 2007.
[40] A. P. Prudnikov, *Integrals and Series*, vol. 3, A. P. Prudnikov, Y. A. Brychkov, O. I. Marichev, and G. G. Gould, Eds. New York, NY, USA: Gordon and Breach, 1998.
[41] E. Basar, I. Yildirim, and F. Kilinc, "Indoor and outdoor physical channel modeling and efficient positioning for reconfigurable intelligent surfaces in mmWave bands," 2020, *arXiv:2006.02240*. [Online]. Available: http://arxiv.org/abs/2006.02240
[42] E. Basar, I. Yildirim, and I. Akyildiz, "Reconfigurable intelligent surfaces for future wireless networks: A channel modeling perspective," 2020, *arXiv:2008.01448*. [Online]. Available: http://arxiv.org/abs/2008.01448

BA CAO NGUYEN received the B.S. degree from Telecommunication University, Khanh Hoa, Vietnam, in 2006, the M.S. degree from the Posts and Telecommunications Institute of Technology (VNPT), Ho Chi Minh City, Vietnam, in 2011, and the Ph.D. degree from Le Quy Don Technical University, Hanoi, Vietnam, in 2020. He currently works as a Lecturer with Telecommunications University. His research interests include energy harvesting, full-duplex, spatial modulation, NOMA, MIMO, RIS, and cooperative communication.

TRAN MANH HOANG received the B.S. degree in communication command from Telecommunications University, Ministry of Defense, Vietnam, in 2002, the B.Eng. degree in electrical engineering from Le Quy Don Technical University, Hanoi, Vietnam, in 2006, the M.Eng. degree in electronics engineering from the Posts and Telecommunications Institute of Technology, (VNPT), Vietnam, in 2013, and the Ph.D. degree from Le Quy Don Technical University, Hanoi, in 2020. He currently works as a Lecturer with Telecommunications University, Khanh Hoa, Vietnam. His research interests include energy harvesting, non-orthogonal multiple access, and signal processing for wireless cooperative communications.

PHUONG T. TRAN (Senior Member, IEEE) was born in Ho Chi Minh City, in 1979. He received the B.Eng. and M.Eng. degrees in electrical engineering from Ho Chi Minh University of Technology, Ho Chi Minh City, Vietnam, in 2002 and 2005, respectively, and the M.S. degree in mathematics and the Ph.D. degree in electrical and computer engineering from Purdue University, in 2013. He became a Vietnam Education Foundation Fellow with Purdue University, USA, in 2007. He joined the Faculty of Electrical and Electronics Engineering, Ton Duc Thang University, Vietnam, in 2013, where he has been working as the Vice Dean, since October 2014. His research interests include wireless communications and network information theory.

TAN N. NGUYEN (Member, IEEE) was born in Nha Trang City, Vietnam, in 1986. He received the B.S. degree in electronics from Ho Chi Minh University of Natural Sciences, in 2008, the M.S. degree in telecommunications engineering from Vietnam National University, in 2012, and the Ph.D. degree in communications technologies from the Faculty of Electrical Engineering and Computer Science, VSB–Technical University of Ostrava, Czech Republic, in 2019. He joined the Faculty of Electrical and Electronics Engineering, Ton Duc Thang University, Vietnam, in 2013, and since then has been lecturing. His major research interests include cooperative communications, cognitive radio, physical layer security, and signal processing.

VAN-DUC PHAN received the M.S. degree from the Department of Electric, Electrical and Telecommunication Engineering, Ho Chi Minh City University of Transport, Ho Chi Minh, Vietnam, and the Ph.D. degree from the Department of Mechanical and Automation Engineering, Da-Yeh University, Taiwan, in 2016. His research interests include sliding mode control, non-linear systems or active magnetic bearing, energy harvesting enabled cooperative networks, improving the optical properties, lighting performance of white LEDs, energy efficiency LED driver integrated circuits, and novel radio access technologies.

BUI VU MINH graduated in electrical and electronic engineering from Nguyen Tat Thanh University, Ho Chi Minh City, Vietnam, in 2015. He received the master's degree in electrical engineering from Ho Chi Minh City University of Technology and Education, Ho Chi Minh City. End of 2014, he joined the Faculty of Mechanical, Electrical, Electronic and Automotive Engineering, Nguyen Tat Thanh University, as a Laboratory-Practice Management, where he was a Lecturer, in 2017. His research interests include artificial neural networks and wireless networks.

MIROSLAV VOZNAK (Senior Member, IEEE) received the Ph.D. degree in telecommunications from the Faculty of Electrical Engineering and Computer Science, VSB–Technical University of Ostrava, in 2002, and the Habilitation degree, in 2009. He was appointed as a Full Professor of electronics and communications technologies, in 2017. He has authored or coauthored over 100 articles indexed in SCI/SCIE journals. According to the Stanford University study released in 2020, he is one of the World's Top 2% of scientists in networking and telecommunications and information and communications technologies. He participated in six projects funded by EU in programs managed directly by European Commission. His research interests include ICT, especially on quality of service and experience, network security, wireless networks, and big data analytics. He is also a Principal Investigator in the research project QUANTUM5 funded by NATO, which focuses on the application of quantum cryptography in 5G campus networks. He served as a General Chair for the 11th IFIP Wireless and Mobile Networking Conference, in 2018, and the 24th IEEE/ACM International Symposium on Distributed Simulation and Real Time Applications, in 2020.